

Design of emitter structures based on resonant perfect absorption for thermophotovoltaic applications

Jonathan J. Foley IV,^{1,2,4} Craig Ungaro,³ Keye Sun,³ Mool C. Gupta,^{3,5}
and Stephen K. Gray^{2,6}

¹*Department of Chemistry, William Paterson University, 300 Pompton Road, Wayne, NJ, 07470, USA*

²*Center for Nanoscale Materials, Argonne National Laboratory, 9700 South Cass Avenue, Argonne, IL, 60439, USA*

³*Department of Electrical & Computer Engineering, University of Virginia, Charlottesville, Virginia, 22901, USA*

⁴foleyj10@wpunj.edu

⁵mgupta@virginia.edu

⁶gray@anl.gov

Abstract: We report a class of thermophotovoltaic emitter structures built upon planar films that support resonant modes, known as perfectly-absorbing modes, that facilitate an exceptional optical response for selective emission. These planar structures have several key advantages over previously-proposed designs for TPV applications: they are simple to fabricate, are stable across a range of temperatures and conditions, and are capable of achieving some of the highest spectral efficiencies reported of any class of emitter structure. Utilization of these emitters leads to exceptionally high device efficiencies under low operating temperature conditions, which should open new opportunities for waste heat management. We present a theoretical framework for understanding this performance, and show that this framework can be leveraged as a search algorithm for promising candidate structures. In addition to providing an efficient theoretical methodology for identifying high-performance emitter structures, our methodology provides new insight into underlying design principles and should pave way for future design of structures that are simple to fabricate, temperature stable, and possess exceptional optical properties.

© 2015 Optical Society of America

OCIS codes: (350.6050) Solar energy; (350.4238) Nanophotonics and photonic crystals; (310.4165) Multilayer design; (310.6805) Theory and design.

References and links

1. S. Fan, "Photovoltaics: An alternative 'sun' for solar cells," *Nat. Nanotechnol.* **9**, 92–93 (2014).
2. P. A. Davies and A. Luque, "Solar thermophotovoltaics: brief review and a new look," *Sol. Energ. Mat. Sol. Cells* **33**, 11–22 (1994).
3. P. Bermel, M. Ghebrebrhan, W. Chan, Y. X. Yeng, M. Araghchini, R. Hamam, C. H. Marton, K. F. Jensen, M. Soljacic, J. D. Joannopoulos, S. G. Johnson, and I. Celanovic, "Design and global optimization of high-efficiency thermophotovoltaic systems," *Opt. Express* **18**, A314–A334 (2010).
4. C. Ungaro, S. K. Gray, and M. C. Gupta, "Black tungsten for solar power generation," *Appl. Phys. Lett.* **103**, 071105 (2013).

5. C. Ungaro, S. K. Gray, and M. C. Gupta, "Graded-index structures for high-efficiency solar thermophotovoltaic emitting surfaces," *Opt. Lett.* **18**, 5259–5262 (2014).
6. A. Lenert, D. M. Bierman, Y. Nam, W. R. Chan, I. Celanovic, M. Soljacic, and E. N. Wang, "A nanophotonic solar thermophotovoltaic device," *Nat. Nanotechnol.* **9**, 126–130 (2014).
7. H. Ye, H. Wang, and Q. Cai, "Two-dimensional VO₂ photonic crystal selective emitter," *J. Quant. Spectros. Radiat. Transfer* **158**, 119 – 126 (2015).
8. E. Rephaeli and S. Fan, "Absorber and emitter for solar thermophotovoltaic systems to achieve efficiency exceeding the Shockley-Queisser limit," *Opt. Express* **17**, 15145–15159 (2009).
9. L. M. Fraas, J. E. Avery, and H. X. Huang, "Thermophotovoltaic furnace-generator for the home using low bandgap GaSb cells," *Semicond. Sci. Technol.* **18**, S247 (2003).
10. V. P. Khvostikov, S. V. Sorokina, O. A. Khvostikova, N. K. Timoshina, N. S. Potapovich, B. Y. Ber, D. Y. Kazantsev, and V. M. Andreev, "High-efficiency GaSb photocells," *Physics of Semiconductor Devices* **47**, 307–313 (2013).
11. M. W. Dashiell, J. F. Beausang, H. Ehsani, G. J. Nichols, D. M. Depoy, L. R. Danielson, P. Talamo, K. D. Rahner, E. J. Brown, S. R. Burger, P. M. Fourspring, W. F. Topper, P. F. Baldasar, C. A. Wang, R. K. Huang, M. K. Connors, G. W. Turner, Z. A. Shellenbarger, G. Taylor, L. Jizhong, R. Martinelli, D. Donetski, S. Anikeev, G. L. Belenky, and S. Luryi, "Quaternary InGaAsSb thermophotovoltaic diodes," *IEEE Trans. Electron Dev.* **53**, 2879–2891 (2006).
12. C. A. Wang, H. K. Choi, S. L. Ransom, G. W. Charache, L. R. Danielson, and D. M. DePoy, "High-quantum-efficiency 0.5 eV GaInAsSb/GaSb thermophotovoltaic devices," *Appl. Phys. Lett.* **75**, 1305–1307 (1999).
13. N. P. Sergeant, O. Pincon, M. Agrawal, and P. Peumans, "Design of wide-angle solar-selective absorbers using aperiodic metal-dielectric stacks," *Opt. Express* **17**, 22800–22812 (2009).
14. J. J. Foley, IV, H. Harutyunyan, D. Rosenmann, R. Divan, G. P. Wiederrecht, and S. K. Gray, "When are surface plasmon polaritons excited in the Kretschmann-Raether configuration?" *Sci. Rep.* **5**, 09929 (2015).
15. P. Yeh, *Optical waves in layered media* (Wiley, 2005).
16. J. A. Nelder and R. Mead, "A simplex method for function minimization," *Comp. J.* **7**, 308–313 (1965).
17. J. M. Montgomery and S. K. Gray, "Enhancing surface plasmon polariton propagation lengths via coupling to asymmetric waveguide structures," *Phys. Rev. B* **77**, 125407–125415 (2008).
18. E. D. Palik, *Handbook of optical constants of solids* (Academic Press, 1998).
19. P. B. Johnson and R. W. Christy, "Optical constants of noble metals," *Phys. Rev. B* **6**, 4370 (1972).
20. M. Shimizu, A. Kohiyama, and H. Y. Yugami, "High-efficiency solar-thermophotovoltaic system equipped with a monolithic planar selective absorber/emitter," *J. Photon. Energy* **5**, 053099–53107 (2015).
21. G. V. Naik, J. L. Schroeder, X. Ni, A. V. Kildishev, T. D. Sands, and A. Boltasseva, "Titanium nitride as a plasmonic material for visible and near-infrared wavelengths," *Opt. Mater. Express* **2**, 478–489 (2012).
22. W. Chan, R. Huang, C. Wang, J. Kassakian, J. Joannopoulos, and I. Celanovic, "Modeling low-bandgap thermophotovoltaic diodes for high-efficiency portable power generators," *Solar Energy Materials and Solar Cells* **94**, 509–514 (2010).
23. P. Nagpal, S. E. Han, A. Stein, and D. J. Norris, "Efficient low-temperature thermophotovoltaic emitters from metallic photonic crystals," *Nano Lett.* **8**, 3238–3243 (2008).
24. M. Lim, S. Jin, S. S. Lee, and B. J. Lee, "Graphene-assisted si-insb thermophotovoltaic system for low temperature applications," *Opt. Express* **23**, A240–A253 (2015).

1. Introduction

Solar energy conversion has been explored through direct sunlight to electric conversion via the photovoltaic (PV) effect, and sunlight to heat, which can be efficiently stored for later use and can be converted to electric power. Solar cells based on the PV effect have a theoretical maximum efficiency of about 32% due to the Shockley-Queisser limit. The reason for the low theoretical maximum conversion efficiency of PV cells is that a significant amount of solar light lies at energies outside of the solar cell bandgap. Solar energy in excess of the bandgap is wasted as heat, while solar photons with energies below the bandgap are transmitted rather than absorbed by the cell. In thermophotovoltaic (TPV) systems, incoming energy is used to heat an emitting surface to high temperatures, which results in a large amount of thermal emission from the surface. This thermal emission is then captured by a low-bandgap PV cell where it is turned into electrical energy. Traditional TPV systems use waste heat or a burning fuel to heat the emitter while solar thermophotovoltaic (STPV) systems use concentrated solar energy [1].

Using a STPV system allows broad-spectrum sunlight to be effectively absorbed and converted into heat and then to electrical energy. This allows for energy from the entire solar spec-

trum to be used, resulting in a theoretical maximum efficiency of 85.4% based on the Carnot cycle limit [2]. As a result, STPV systems have the potential to be far more efficient than PV cells. By controlling the optical properties of the STPV emitting surface, its thermal emission can be spectrally matched to a PV cell, resulting in high efficiency operation [3–6]. Perhaps the most impressive emitters to date have exploited optical resonances resulting from patterned surfaces, including a VO₂-based photonic crystal with an optimal spectral efficiency (see Eq. (1)) of 54% for InGaSb PV cells with a band gap of 0.62 eV [7], W-based graded index structure with an optimal efficiency of 59% for GaSb PV cells with a band gap of 0.73 eV [5], and W-based photonic crystals with an optimal efficiency of 63% for GaSb PV cells with a band gap of 0.73 eV [8]. However, these structures suffer from several key drawbacks: they typically rely on precise fabrication of sub-wavelength structures to tune their resonant properties, and they require high operating temperatures to achieve high spectral efficiencies. For example, the spectral efficiency of the VO₂ photonic crystal drops from 54% to 41% if the operating temperature is lowered from the optimal 1500 K to 1300 K [7]. The requisite high operating temperatures means these structures are susceptible to deformation during operating conditions, which can compromise their resonant properties and severely degrade their performance. Their low-efficiency at low temperatures precludes their application to a number of potential waste heat reclamation technologies.

In this work, we present a theoretical framework for a phenomenon known as resonant perfect absorption that can be leveraged for the design of simple planar emitter structures that have the highest reported spectral efficiencies to our knowledge. These planar structure have several key advantages over previously-proposed structures for TPV applications: they are simple to fabricate, are stable across a range of temperatures and conditions, and can be used to achieve high conversion efficiencies even at low operating temperatures. We also provide experimental validation for our designs by fabricating and characterizing an emitter structure based on this methodology. In addition to providing an efficient theoretical methodology for identifying high-performance emitter structures, our methodology provides new insight into underlying design principles and should pave way for future design of structures that are simple to fabricate, temperature stable, and possess exceptional optical properties. The exceptional performance of devices utilizing these emitter structures at low (1000 K) temperatures should open new opportunities for waste heat management.

2. Spectral efficiency

Emitter structures are often characterized by their spectral efficiency (SE), which reports the fraction of the absorbed energy emitted by the selective emitter that a PV cell is able to use. The total available emitted spectral energy is found by multiplying the emittance by the blackbody thermal radiation spectrum. In this work, we consider the spectral efficiency of structures for two PV cells common in TPV systems: GaSb with a bandgap of 0.7326 eV ($\lambda_{bg} = 1707$ nm) and InGaAsSb with a bandgap of 0.550 eV ($\lambda_{bg} = 2254$ nm) [9–12]. High (1750 K) and low (1000 K) temperature conditions are considered.

The spectral efficiency is given by [5]

$$SE = \frac{\int_0^{\lambda_{bg}} \frac{E_{bg}}{E_\lambda} B(\lambda, T) \varepsilon_S(\lambda) d\lambda}{\int_0^\infty B(\lambda, T) \varepsilon_S(\lambda) d\lambda} \quad (1)$$

where E_{bg} is the bandgap energy of the PV cell, E_λ is the energy of a photon with wavelength λ , $B(\lambda, T)$ is Planck's law for blackbody radiation, and $\varepsilon_S(\lambda)$ is the spectral emittance of the surface. High SE emitters tend to have negligible emittance at wavelengths longer than λ_{bg} and near-unity emittance at or just short of λ_{bg} . While a spectrally narrow emission is desired

to reduce thermalization loss in the PV cell, some bandwidth is required to increase the power density of the emitted radiation. Systems with extremely narrow emission require a large emitter area, which results in a large PV cell area requirement and a greatly increased system cost [3–6].

3. Resonant perfect-absorption in planar structures

If the emissivity of the emitter structure can be expressed simply in terms of its geometry and material parameters, then the spectral efficiency may be viewed as an objective function, and an optimization can be performed in terms of these variables. For example, this concept has been used to design planar structures for TPV absorbers and emitters, where the spectral efficiency objective function is optimized using derivative-less techniques like the Nelder-Mead method [13]. This approach can also be used to design more complicated structures, such as the 2-D photonic crystal described in reference [8], but analytical methods are no longer appropriate for computation of the emissivity to update the objective. In this case, the numerical optimization must also be coupled to numerical electrodynamics techniques, which increases the computational cost. An important drawback of this approach is that in all cases, it is unclear how to uncover design principles for promising structures without first identifying a concrete physical phenomenon that gives rise to high spectral efficiency.

We have recently developed a theoretical framework for a physical phenomenon in simple planar structures, known as resonant perfect absorption, that leads to the optical response requisite for high spectral efficiency [14]. Here we demonstrate that this theoretical framework provides predictive power for the design of high spectral efficiency emitter structures, and also provides insight that can guide their further improvement. Optimizing over spectral efficiency, which lacks clear necessary conditions for optimality, is replaced by locating zeros in the reflectance amplitude, which are well defined in terms of a complex wavevector values that define perfectly absorbing modes. We demonstrate this predictive power by using this framework to identify simple planar structures that show an exceptional spectral efficiency of nearly 70%. The simplicity of the structures designed by our methodology is amenable to simple fabrication processes, which allows us to easily validate our predictions experimentally.

Electromagnetic waves supported by a general L -layer structures must satisfy appropriate boundary conditions, which are written concisely in the matrix form introduced by Yeh [15],

$$\begin{pmatrix} E_1^+ \\ E_1^- \end{pmatrix} = \begin{pmatrix} M_{1,1} & M_{1,2} \\ M_{2,1} & M_{2,2} \end{pmatrix} \begin{pmatrix} E_L^+ \\ E_L^- \end{pmatrix}, \quad (2)$$

where the precise value of the matrix elements $M_{i,j}$ depend on the thickness and refractive index of each layer in the multi-layer structure, as well as the frequency, polarization, and (complex) wavevector of light, see Appendix for more details. Resonant perfect absorption in these structures can be understood in terms of modes in these structures, known as perfectly absorbing (PA) modes. PA modes are defined as solutions to the above matrix equation when E_1^- and E_L^+ are set to zero, which is satisfied when $M_{2,1} = 0$. [14] By definition of the Fresnel reflection amplitude, $r = M_{2,1}/M_{1,1}$, we see that the reflection on resonance with the PA mode is rigorously zero. In this work, we confine our attention to structures terminated by an optically-thick metal substrate, meaning transmission through these structures is also necessarily zero. Hence absorption, and emission at thermal equilibrium, are indeed perfect for the PA modes in these structures. Because they are resonant modes, they have the potential to impart selective spectral emission requisite for high efficiency TPV emitter structures.

Recalling that the matrix elements depend on the geometry as well as the wavevector, we formulate the modal equations as a search for $M_{2,1}(\omega, \alpha, \beta, \mathbf{d}) = 0$, where β and α denote the real and imaginary components of the optical wavevector, respectively. The vector \mathbf{d} denotes the vector of thicknesses of each planar film, which completely defines the geometry of the

structure so long as the composition of each layer is specified. The wavevector components β can be related to an angle of incidence that is resonant with the PA mode, specifically $\beta = n_i k_0 \sin(\theta_i)$, where k_0 is the free-space wavevector and n_i is the refractive index of the material through which light is incident, typically air. While a similar interpretation is possible for the imaginary wave-vector component, a more physically concrete interpretation is that it relates to the resonance line-width of the PA mode. In either interpretation, a smaller α magnitude is desirable for TPV applications because it indicates that the PA modes can be efficiently coupled into by light at real angles of incidence, and that the resonance line-width is relatively narrow, which are both desirable from the point of view of spectral efficiency. We also desire that β be close to zero so that normally-incident light can couple efficiently into the PA mode.

With this in mind, we can design a search routine using standard numerical methods to locate structures that support PA modes in the frequency range of our choice that also have magnitudes of β and α that are relatively small [14, 16, 17]. That is, for the InGaAsSb PV cells, we can search for 2- and 4-layer structures that support PA modes in the energy window slightly higher than 0.55 eV, and for GaSb PV cells, we search for 2- and 4-layer structures that support PA modes in the energy window slightly higher than 0.72 eV. Such a search can be used to hone in on structures that show considerable promise for TPV applications. Further refinement can be performed on these candidate structures by optimizing over the FOM defined by Eq. (1) where the emissivity is computed simply from the Fresnel equations and the Blackbody spectrum corresponds to the temperature of interest. While in this work, we will focus exclusively on planar structures, we note that resonant perfect absorption can occur in higher dimensional photonic crystals. The methodology we outline can therefore be generalized to these structures, though numerical electrostatics techniques may be required to compute the photonic band structure.

4. Results

We follow the procedure outlined above to locate geometries of 2- and 4-layer planar structures. For 2-layer structures, layer 1 functions as a dielectric anti-reflective coating and layer 2 is an optically-thick absorbing layer. For 4-layer structures, layers 1 and 3 are dielectric layers, while layers 2 and 4 are absorbing layers. Layer 4 is again optically-thick, while layer 2 is a thin film (see Fig. 1 inset and Fig. 2(c) for a schematics). Silver and tungsten are considered for the absorbing layers, and yttria-stabilized zirconia (YSZ) is used for the dielectric layers. We assume a refractive index of 2.1 for YSZ and take the permittivity of W from reference [18] and the permittivity of Ag from reference [19].

We perform searches for PA modes as described in the previous section. For 4-layer structures, we allow d_1 , d_2 , and d_3 (the thicknesses of layers 1, 2, and 3, respectively) to vary, while for 2-layer structures, we allow only d_1 (dielectric over-layer) to vary. We first confine our attention to energy ranges between 0.73 and 0.85 eV (λ between 1450 and 1700 nm, or 3.69 to $4.33 \mu\text{m}^{-1}$) to target emitters for GaSb cells. If we confine our search to ranges of the modal wavevector magnitude less than or equal to $1 \mu\text{m}^{-1}$, we can consider our search as confined to a reciprocal volume of about $0.64 \mu\text{m}^{-3}$. A particularly high density of PA modes can be found in this reciprocal volume for structures of the type YSZ/Ag/YSZ/W and YSZ/W/YSZ/W, while the density of PA modes in this reciprocal volume for YSZ/W/YSZ/W and YSZ/Ag/YSZ/Ag are considerably lower. Furthermore, we find no PA modes can be found within the light line for 2-layer structures of YSZ/W or YSZ/Ag. Of the two structures with a highest density of PA modes in the reciprocal volume of interest, we see that YSZ/Ag/YSZ/W has considerably more PA modes with $\beta < 0.1 \mu\text{m}^{-1}$, indicating that normally incident light can couple very efficiently to these modes. In particular, we see from this modal search that structures with d_1 in the range 100-150 nm, d_2 in the range 10 to 20 nm, and d_3 in the range 250 to 300 nm can

support PA modes with small β and α in the frequency range of interest.

This process is repeated to target structures for InGaAsSb cells, this time confining the search to energy ranges between 0.55 and 0.65 eV (λ between 1900 and 2254 nm). From this search, we see a high density of modes with small β and α when d_1 is in the range 130-170 nm, d_2 is in the range 16-30 nm, and d_3 is in the range 350-470 nm.

Table 1. Geometries, spectral efficiencies, and device efficiencies of structures optimized for $\lambda_{bg} = 2254$ nm and $\lambda_{bg} = 1707$ nm, for low- (1000 K) and high-temperature (1750 K) operation. We compare 4-layer structures to 2-layer structures. For 4-layer structures, d_1 is the thickness of a dielectric coating, d_2 is the thickness of a thin metal film, d_3 is the thickness of the dielectric spacer on top of an optically-thick tungsten substrate. For 2-layer structures, d_3 is the thickness of a dielectric coating on top of optically-thick tungsten.

$\lambda_{bg} = 2254$ nm at 1000 K					
Structure	d_1 (nm)	d_2 (nm)	d_3 (nm)	Spec. Eff. (%)	Sys. Eff. (%)
Si ₃ N ₄ /Ag/Si ₃ N ₄	167	14	456	45.7	9.7
YSZ/Ag/YSZ	148	15.5	393	47.8	10.0
Si ₃ N ₄ /W/Si ₃ N ₄	169	48	369	42.2	9.5
YSZ/W/YSZ	148	52	314	43.7	9.8
Si ₃ N ₄ /Ta/Si ₃ N ₄	178	24	440	35.2	7.7
YSZ/Ta/YSZ	154	22	345	39.5	8.6
Si ₃ N ₄ /W	0	0	167	39.7	7.1
YSZ/W	0	0	146	41.4	8.3
Bare W	0	0	0	31.1	3.6
$\lambda_{bg} = 1707$ nm at 1000 K					
Si ₃ N ₄ /Ag/Si ₃ N ₄	129	13	335	34.4	5.7
YSZ/Ag/YSZ	115	14	288	36.2	5.9
Si ₃ N ₄ /W/Si ₃ N ₄	132	60	16	24.6	5.4
YSZ/W/YSZ	113	60	16	25.6	5.6
Si ₃ N ₄ /Ta/Si ₃ N ₄	137	24	316	20.9	4.7
YSZ/Ta/YSZ	118	25	266	22.2	5.2
Si ₃ N ₄ /W	0	0	133	24.8	4.7
YSZ/W	0	0	115	25.8	5.3
$\lambda_{bg} = 2254$ nm at 1750 K					
YSZ/Ag/YSZ	175	20	389	65.2	16.8
YSZ/Ta/YSZ	156	23	321	59.5	17.0
YSZ/W/YSZ	159	47	288	60.2	17.1
YSZ/W	0	0	160	58.3	16.9
$\lambda_{bg} = 1707$ nm at 1750 K					
YSZ/Ag/YSZ	126	19	283	68.0	20.8
YSZ/Ta/YSZ	107	27	244	56.2	19.8
YSZ/W/YSZ	105	60	16	57.0	20.2
YSZ/W	0	0	104	57.3	20.3

We further refine our structures by optimizing Eq. (1) over \mathbf{d} for a given band-gap energy and temperature. We first fix the temperature at 1000 K for optimizations for InGaAsSb and GaSb cells. Indeed, the performance of YSZ/Ag/YSZ/W structures optimized for this low-

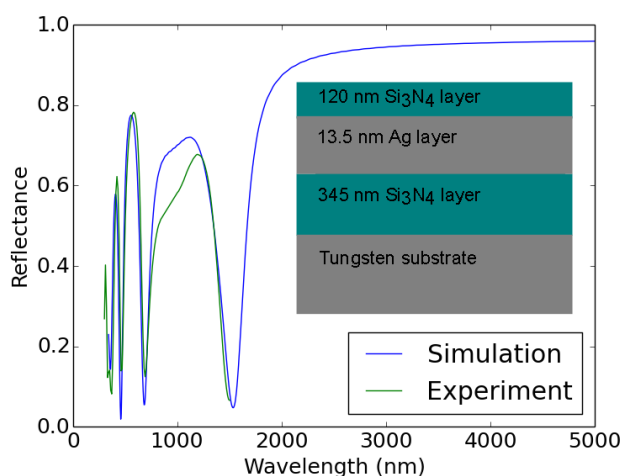


Fig. 1. Comparison of simulated and experimental results for the reflectance of a sample with a d_1 of 120 nm, a d_2 of 13.5 nm, and a d_3 of 345 nm. **Inset:** The fabricated structure.

temperature operation is quite impressive for low temperature conditions, giving SE of about 48% for InGaAsSb cells and 37% for GaSb cells (see Table I). This is particularly impressive considering that this structure's spectral efficiency at 1000 K is 13.5% higher than the that of the 2-D photonic crystal at 1300 K described in [7], Ye *et al.* Maps of the emissivity of these structures as a function of wavelength and angle are given in Fig. 2, as well as a schematic of the structure geometry. An important feature of the optical response of these structures is that the frequency of the emissivity maxima is relatively angle-insensitive. This can again be related to features of the PA modes, in particular, their dispersion. In Fig. 5 in the Appendix we show the PA dispersion for several structures optimized for the InGaAsSb cells at 1000 K operation and see that the PA dispersions at around 0.55 eV are relatively flat, which accounts for the lack of strong angular dependence of the emissivity peak. Compared to the YSZ/Ag/YSZ/W structures, we find that optimized YSZ/W/YSZ/W structures, which were recently discussed by Shimizu, Kohiyama, and Yugami for higher (1650 K) operation [20], perform considerably worse, with spectral efficiencies that are lower by 11% and 29% for InGaAsSb and GaSb cells, respectively. In fact, the performance of tungsten with an optimized anti-reflective coating can essentially match the performance of the more complicated YSZ/W/YSZ/W structure seen in reference [20] (see Table I). The optical response of YSZ/W and YSZ/W/YSZ/W structures differs markedly from the YSZ/Ag/YSZ/W structure, as can be seen by the emissivity curves of the optimized structures (see Table I for optimal geometries). In Fig. 3(a), we plot the emissivity of these structures optimized for InGaAsSb cells at 1000 K operation, and note the near perfect emissivity that is observed at $\lambda = 2\mu\text{m}$ in the YSZ/Ag/YSZ/W structure. Under these operation conditions, the various structures in fact give fairly similar spectral efficiencies despite having qualitatively different emissivities. However, the perfect absorption/emissivity feature of the YSZ/Ag/YSZ/W structure shows exceptional tunability (see Fig. 2), which allows this structure to be simply modified to give superior performance for a variety of PV materials and operating conditions. If we examine the PA modes for this YSZ/Ag/YSZ/W, we see indeed that β is nearly zero, indicating normally incident light can couple efficiently into this mode (see Fig. 3(b)). On the other hand, β is fairly large for PA modes in YSZ/W and YSZ/W/YSZ/W, indicating that normally incident light cannot couple efficiently to these modes (see Fig. 6 in the Appendix).

We consider substituting tantalum for layer 2 in the base structure from the modal search, i.e. YSZ/Ta/YSZ/W, but find that performance is generally lower than structures with either W or Ag. The results are much less sensitive to substitution of the dielectric material. For example, using Si₃N₄, another common dielectric material for high-temperature applications, for layer 1 and 3 yields results quite similar to those when YSZ is used. We find that structures can be optimized with Si₃N₄ to give nearly the same spectral efficiencies, although the dielectric layers are generally thicker to achieve comparable optical path lengths, as we take the refractive index of Si₃N₄ to be 1.8. These results suggest that the nature of the PA modes can be tuned dramatically by changing the properties the thin-film absorbing layer. Ideally, the wavevector of the mode should approach zero. A map of α and β as a function of permittivity for PA modes at an energy well matched to the GaSb cell suggests that thin-films that are good plasmonic materials are ideal for these applications (see Fig. 7 in the Appendix). Recent investigations on the plasmonic properties of temperature-stable ceramics like titanium nitride may therefore offer promising materials for constructing high-efficiency emitter structures based on resonant perfect absorption [21].

To further demonstrate the robust performance of the YSZ/Ag/YSZ/W structure, we optimize over \mathbf{d} for both PV cells assuming an operating temperature of 1750 K, giving a spectral efficiency of 68% and 65% for GaSb and InGaAsSb cells, respectively (see Table I). Indeed, this exceeds what is, to our knowledge, the highest reported spectral efficiency for GaSb cells by more than 7% with a much simpler design [8]. Here, the YSZ/W/YSZ/W structures discussed in reference [20] have optimal spectral efficiencies that are 16% and 8% lower for GaSb and InGaAsSb cells, respectively. Interestingly again, the optimized 4-layer structure consisting of YSZ/W/YSZ/W performs comparably to a simple W substrate with an optimized YSZ anti-reflective coating (see Table I).

Table 2. Geometries and output power densities of emitter structures. We compare highly selective 4-layer emitter structures (YSZ/Ag/YSZ/W) to broad-band 2-layer structures (YSZ/W). For the 4-layer structures, d_1 is the thickness of YSZ, d_2 is the thickness of Ag, and d_3 is the thickness of the YSZ spacer layer on top of an optically-thick tungsten substrate. For the 2-layer structures, d_3 is the thickness of a YSZ coating on top of optically-thick tungsten. Geometries are taken from the structures given in Table 1.

$\lambda_{bg} = 2254 \text{ nm at } 1000 \text{ K}$				
Structure	d_1 (nm)	d_2 (nm)	d_3 (nm)	Output Power Density W/m ²
YSZ/Ag/YSZ	148	15.5	393	1,567
YSZ/W	0	0	146	1,707
$\lambda_{bg} = 1707 \text{ nm at } 1000 \text{ K}$				
YSZ/Ag/YSZ	115	14	288	897
YSZ/W	0	0	115	921
$\lambda_{bg} = 2254 \text{ nm at } 1750 \text{ K}$				
YSZ/Ag/YSZ	175	20	389	35,654
YSZ/W	0	0	160	81,273
$\lambda_{bg} = 1707 \text{ nm at } 1750 \text{ K}$				
YSZ/Ag/YSZ	126	19	283	43,400
YSZ/W	0	0	104	77,043

A further quantity of interest for assessing the performance of emitter structures for STPV/TPV applications is the output power density, the power radiated by an emitter structure

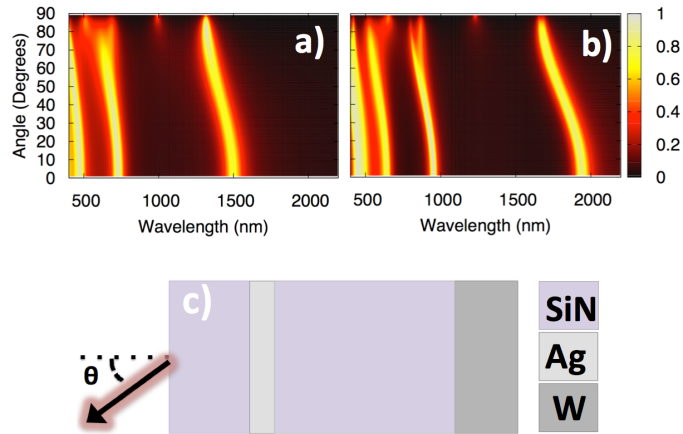


Fig. 2. Maps of Emissivity as a function of emission angle and wavelength. **a)** Emissivity map of thin-film structure optimized for PV material with $\lambda_{bg} = 1707$ nm with an operating temperature of 1000 K. **b)** Emissivity map of thin-film structure optimized for PV material with $\lambda_{bg} = 2254$ nm with an operating temperature of 1000 K. **c)** Schematic of emitter structure consisting of an optically-thick tungsten substrate with thin-film layers of Ag and Si_3N_4 to mediate selective absorption/emission.

per unit area of the structure, in the spectral range of interest. The cutoff of the spectral range for STPV/TPV applications is determined by the PV bandgap, and the output power density can be computed simply from the numerator of Eq. (1). While the spectral efficiency as a figure of merit tends to favor highly selective emitter structures, broad-band emitters will tend to have higher output power densities for the same operating conditions. In Table 2, we compare the output power densities of highly selective (YSZ/Ag/ISA/W) emitter structures to broad-band (YSZ/W) emitter structures. For high operating temperatures (1750 K), the broad-band emitter structures have significantly higher output power densities than the highly selective emitter structures (about 80% and 130% higher for use with GaSb and InGaAsSb cells, respectively). However, these margins are much less dramatic at low operating temperatures (1000 K), where the broad-band emitters have output power densities that are about 3% and 9% higher than the highly selective emitters for use with GaSb and InGaAsSb cells, respectively. This suggests a potential advantage for using the theory of resonant perfect absorption as a framework for designing emitter structures for low-temperature operating conditions, especially given the exceptionally high spectral and system efficiencies predicted for these structures in Table 1.

The reflectance of fabricated and simulated structures are compared in Fig. 1 for a sample with a d_1 of 120 nm, a d_2 of 13.5 nm, and a d_3 of 345 nm. The FOM of this structure is 0.56 at 1750 K. Excellent agreement is found between these results, which serves both to validate the theoretical predictions and demonstrate the feasibility of fabricating structures to within the specifications required to achieve high spectral efficiencies. The discrepancy between simulated and experimental results in the 800 to 1200 nm range is due to a lamp change in the spectrometer in this region.

The fabrication procedure is straightforward and easy to implement. Double-side polished tungsten (W) substrates were purchased from MTI Corporation. Substrates were cleaned by acetone and methanol sequentially. Stacks of silicon nitride (Si_3N_4) and silver (Ag) layers were deposited onto the W substrates. The structure is analogous to the schematic shown in Fig. 2. The Si_3N_4 layers were deposited by plasma-enhanced chemical vapor deposition (PECVD).

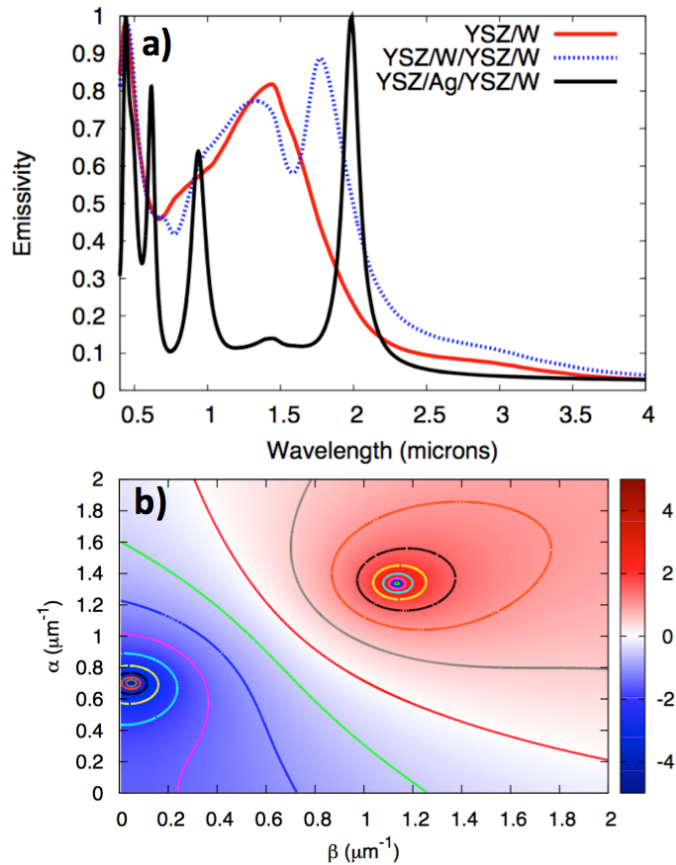


Fig. 3. **Top** Emissivity of various structures optimized for InGaAsSb cells. **Bottom** Reflectance in the complex β, α plane for optimized YSZ/Ag/YSZ/W structure at $\lambda = 2\mu\text{m}$. We see that the strong emissivity peak of the YSZ/Ag/YSZ/W structure corresponds to resonant perfect absorption.

The deposition temperature was kept at 100°C . The Ag layer was deposited by e-beam evaporation. The reflection of the coating was measured by a spectrometer (PerkinElmer, Lambda 950 UV/VIS).

The total power conversion efficiencies for cylindrical STPV systems utilizing the structures outlined in this paper are also shown in Table I. These were calculated assuming a blackbody (absorbance = 0.99) absorber, and solar concentration ratio of $C = 1000$ for the low (1000 K) temperature systems, and $C = 2500$ for the high (1750 K) temperature systems. GaSb PV cells with an E_{bg} of 0.72 eV, fill factor of 0.82, V_{oc} of .55, and EQE of 0.7 and InGaAsSb PV cells with an E_{bg} of 0.55 eV, fill factor of .74, V_{oc} of .4, and EQE of .56 were used in these simulations [6, 10, 22]. The simulations show that a high system efficiency can be obtained using the simple structures outlined in this paper. They also show that high efficiencies can be maintained at lower operating temperatures by changing the parameters of the coatings used in the emitting structures. Low temperature TPV structures are of great interest for waste-heat reclamation [23, 24].

We presented a theoretical framework for a phenomenon known as resonant perfect absorp-

tion that can be leveraged for the design of high spectral-efficiency emitter structures. This framework guided the design of a simple class of emitter structures built upon planar films that support perfectly absorbing (PA) modes. In particular, we found that structures composed of YSZ/Ag/YSZ/W support PA modes with particularly favorable characteristics for TPV applications. Importantly, this structure is robust to substitutions of the dielectric material, which we demonstrate by comparing the performance of $\text{Si}_3\text{N}_4/\text{Ag}/\text{Si}_3\text{N}_4/\text{W}$ structures. Further refinement of the structure, taking into account key parameters like temperature, is possible using the spectral efficiency as an optimization objective. Following this procedure, we obtain structures that have exceptionally high spectral efficiencies across a range of operating temperatures. That these simple planar structure can achieve such high spectral efficiencies is advantageous from the point of view of fabrication feasibility and temperature stability. Although the low melting temperature of Ag precludes its use in emitters designed for high-temperature operation, our high-temperature results illustrate the utility of using the theory of resonant perfect absorption as a tool for designing high-performance emitter structures. In particular, these results may be of practical value if our approach is applied to the design of structures containing plasmonic materials, which have been shown to have tunable optical properties and sufficient temperature stability for TPV applications [21]. A further advantage of our approach is that it identifies a concrete physical phenomenon, resonant perfect absorption, that provides the basis for the exceptional performance of these emitter structures, as well as a predictive theoretical framework for identifying structures that support perfectly absorbing modes. Hence our methodology provides new insight into underlying design principles and should pave way for future engineering of structures that are simple to fabricate, temperature stable, and possess exceptional optical properties.

Appendix

Boundary conditions of electromagnetic waves in planar structures

Consider an L-layer system, with Figure 4 depicting the $L = 4$ case. The optical response in each layer j arises from the (in general) frequency-dependent refractive index, $N_j(\omega) = n_j(\omega) + ik_j(\omega)$, where n_j and k_j are real numbers. The associated electrical permittivity is $\epsilon_j = N_j^2$. Layers $j = 1$ and $j = L$ are semi-infinite, generally non-absorbing dielectric materials characterized by real, positive refractive indices, $N_1 = n_1 > 0$ and $N_L = n_L > 0$. The central layers $2, \dots, L-1$ could include absorbing materials that are described by complex refractive indices. Metallic layers are absorbing but can also be such that $\text{Re}(\epsilon_j) = \text{Re}(N_j^2) = n_j^2 - k_j^2 < 0$. Since the films, with our coordinate system choice (Fig. 4), are homogeneous in the y -direction, the relevant tangential electrical field component is taken to be the real part of the phasor $\exp(i(k_x x - \omega t)) E(z)$ with [1,2]

$$E(z) = \begin{cases} E_1^+ \exp(ik_{z1}z) + E_1^- \exp(-ik_{z1}z) & z < z_1 \equiv 0 \\ E_2^+ \exp(ik_{z2}(z - z_1)) + E_2^- \exp(-ik_{z2}(z - z_1)) & z_1 < z < z_2 \\ \dots & \\ E_L^+ \exp(ik_{zL}(z - z_{L-1})) + E_L^- \exp(-ik_{zL}(z - z_{L-1})) & z > z_{L-1} \end{cases}$$

where the z -component of the wavevector in each layer satisfies

$$k_{zj} = \pm \sqrt{N_j^2 k_0^2 - k_x^2} \quad , \quad (3)$$

with $k_0 = \omega/c$. For p -polarized light $E(z) \equiv E_x(z)$, and for s -polarized light $E(z) \equiv E_y(z)$.

The boundary conditions for satisfying Maxwell's equations are that the tangential components of the magnetic (and electric) field be continuous across each interface, which leads to

[1]:

$$\begin{pmatrix} E_1^+ \\ E_1^- \end{pmatrix} = D_1^{-1} D_2 \begin{pmatrix} E_2^+ \\ E_2^- \end{pmatrix}$$

and

$$\begin{pmatrix} E_l^+ \\ E_l^- \end{pmatrix} = P_l D_l^{-1} D_{l+1} \begin{pmatrix} E_{l+1}^+ \\ E_{l+1}^- \end{pmatrix}$$

for $l = 1, \dots, L-1$. The matrix D_l is defined

$$D_l = \begin{pmatrix} \cos(\theta_l) & \cos(\theta_l) \\ N_l & -N_l \end{pmatrix}$$

for p -polarized light and

$$D_l = \begin{pmatrix} 1 & 1 \\ N_l \cos(\theta_l) & -N_l \cos(\theta_l) \end{pmatrix}$$

for s -polarized light. For the entire L -layer structure, we have

$$\begin{pmatrix} M_{11} & M_{12} \\ M_{21} & M_{22} \end{pmatrix} = D_1^{-1} \left(\prod_{l=2}^{L-1} D_l P_l D_l^{-1} \right) D_L,$$

where P_l is

$$P_l = \begin{pmatrix} \exp(-ik_{z_l}d_l) & 0 \\ 0 & \exp(ik_{z_l}d_l) \end{pmatrix}.$$

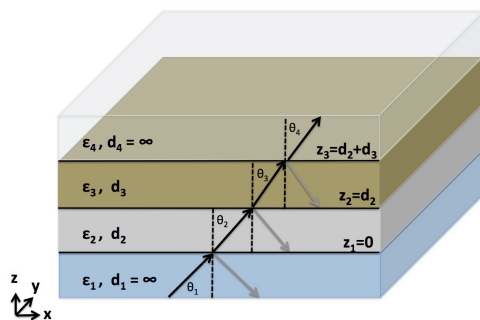


Fig. 4. Schematic of 4 layer system with finite thickness (d_2 and d_3) sandwiched by 2 semi-infinite dielectric layers illustrating coordinate system used for Fresnel equations.

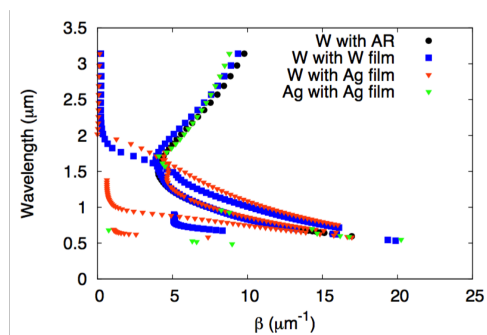


Fig. 5. Dispersion of perfectly absorbing modes in various structures. **W with AR** corresponds to a 2-layer YSZ/W structure. **W with W film** corresponds to a 4-layer YSZ/W/YSZ/W structure. **W with Ag film** corresponds to a 4-layer YSZ/Ag/YSZ/W structure. **Ag with Ag film** corresponds to a 4-layer YSZ/Ag/YSZ/Ag structure. At critical frequencies, the YSZ/Ag/YSZ/W structure supports perfectly absorbing modes with low β and α , indicating that normally-incident light couples efficiently into these modes.

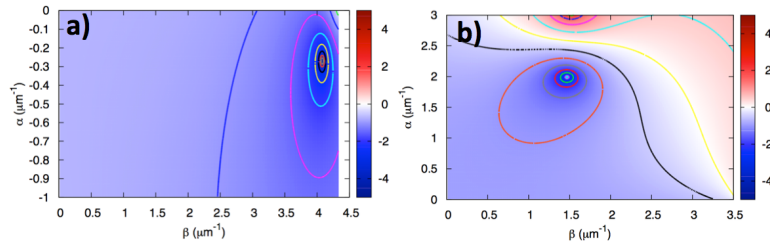


Fig. 6. Reflectance in the complex wavevector plane near perfectly absorbing resonances. Reflectance plane near PA resonance for **a)** YSZ/W structure and **b)** YSZ/W/YSZ/W structure optimized for InGaAsSb cells at 1000K operation, see Table I in the main text for geometries.

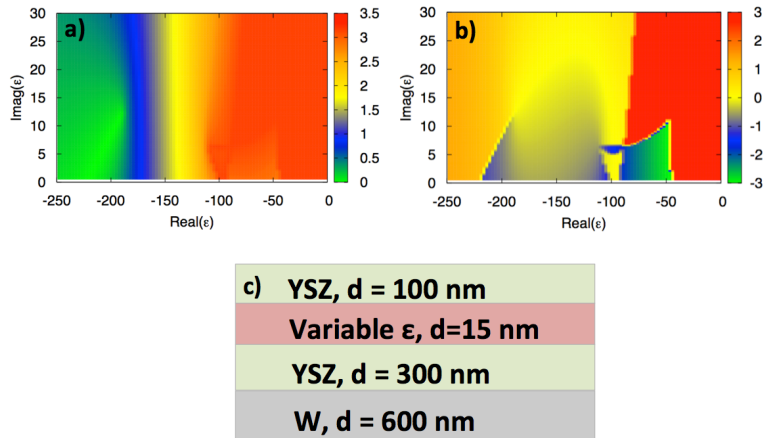


Fig. 7. Map of the β (panel **a**) and α (panel **b**) defining the PA modes in a hypothetical structure illustrated in panel **c**). For this structure, we fix the geometries of all layers as illustrated. We use a permittivity value of 4.41 for layers 1 and 3 (corresponding to YSZ), and a permittivity value of $-56.13 + 19.25i$ for layer 4 (corresponding to Tungsten at $2 \mu\text{m}$). The modal equations are scanned for values of $\text{Re}(\epsilon)$ in the range of -250 to 0 and $\text{Im}(\epsilon)$ in the range 0.5 to 30 with k_0 fixed at $3.14 \mu\text{m}$, yielding a map of the β and α values, note that α can have both positive and negative values. This calculation reveals that in general, large negative values of $\text{Re}(\epsilon)$ and small values of $\text{Im}(\epsilon)$ give rise to PA modes in this structure with small β and α values, meaning that normally incident light can couple efficiently to these modes and that these modes have narrow resonance features.

Acknowledgments

This work was performed at the Center for Nanoscale Materials, a U.S. Department of Energy, Office of Science, Office of Basic Energy Sciences User Facility under Contract No. DE-AC02-06CH11357. We would also like to thank the NASA Langley Professor and NSF IUCRC programs for their support of this project. *JJF and CU contributed equally.